Analysis of a localized flash-flood event over the central Mediterranean

E. Gascón[a,*], S. Laviola[b], A. Merino[a], M. M. Miglietta[c]

[a]*Atmospheric Physics Group, IMA, University of León, 24071 León, Spain*
[b]*ISAC-CNR, Bologna, Italy*
[c]*ISAC-CNR, Lecce, Italy*

Abstract

On 3 July 2006, an exceptionally heavy convective rainfall affected a small area in Calabria, Italy. A rainfall amount of 202 mm was recorded in 2.5 hours , producing considerable damage and causing a localized flash flood. The Weather Research and Forecasting model (WRF) was used to analyse the instability present in the event and the related triggering mechanisms. The high-resolution simulation is able to correctly identify the position of the precipitation peak and to clarify the mesoscale processes involved, although it significantly underestimates the total amount of precipitation. Some sensitivity experiments confirm the importance of the choice of Planetary Boundary Layer and microphysics parameterization schemes for a correct simulation of the event, showing a strong sensitivity to these numerical tests. Also, the need for high horizontal resolution emerges clearly: an accurate representation of the orography at small scales, is required to simulate the event in its correct location. Instability indices identified an extremely favorable environment for convection development, with very high values of CAPE and high moisture content at low levels. The low mountains near the rainfall peak play an important role in triggering the release of instability and controlling the location of rainfall; in particular, the peculiar morphology of the orography creates low-level wind convergence and provides the uplift necessary for the air parcels to reach the level of free convection. In

*Corresponding author: E. Gascón
Email address: `egass@unileon.es` (E. Gascón)

this framework, nondimensional parameters, such as the Froude number, have been calculated to better understand the interaction of the flow with the orography.

Keywords: heavy rainfall, numerical models, orography, convection, flash flood

1. Introduction

One of the most challenging problems in meteorology is quantitative precipitation forecasting, especially when predicting heavy rain events. Large rainfall amounts could be due to convective cells moving repeatedly along the same track but also to stationary cells, located for instance on the convergence line between a cold pool and the upstream flow (Chappell, 1986). These events, which may induce flash flooding, sometimes producing loss of life and affecting the local economy, are often associated with the orography, which serves as a fixed lifting mechanism to force moist flow to its lifting condensation level and to "anchor" the system. The Mediterranean region is prone to flash floods since littoral and pre-littoral mountain areas favour torrential rain concentrated in small catchments (Llasat et al., 2016). In fact, flash floods are considered the most dangerous meteorological hazards in the Mediterranean due to their high frequency, human activity and number of people affected (Llasat-Botija et al., 2007).

The occurrence of heavy rainfall conducive to flash floods is well documented around the world in regions with complex orography (see for example Pontrelli et al. (1999); Miglietta and Rotunno (2012). In order to better understand the mechanisms of triggering and development of orographic precipitation, a variety of specific observation campaigns have been developed, such as the Mesoscale Alpine Programme (MAP; Rotunno and Houze (2007)), the Convective and Orographically-Induced Precipitation Study (COPS; Wulfmeyer et al. (2011), or the Southwest Monsoon Experiment/Terrain-Influenced Monsoon Rainfall Experiment (SoWMEX/TiMREX; Davis and Lee (2012)). Also, the recent HYdrological cycle in the Mediterranean EXperiment (HyMeX, http://www.hymex.org; Ducrocq et al. (2014)) aims at improving the scientific knowledge of the water cycle variability in a region with rough orography like the Mediterranean basin.

Delrieu et al. (2005) summarized the conditions necessary for potentially dangerous flash flood episodes at different scales: a deep and sustained source of heat and moisture, such as the Mediterranean Sea, especially at the end of summer or the beginning of autumn, when the sea is still warm and the intrusions of colder air are more frequent; a large-scale mechanism of convergence and lifting, e.g. provided by a deep upper-level cold trough, which is a typical feature in most Mediterranean storms; the presence of significant orography next to the sea, as in the Mediterranean region, which acts as triggering mechanism of convection and deflects the low-level flows inducing local convergence, which may locally cause the release of instability and induce heavy rainfall (Altinbilek et al., 1997). The influence of the orography is sometimes very localized, so that even very small scale features can play an important role (Gheusi and Stein, 2003). To improve the prediction of heavy rain events we need, on one hand, to understand the mechanisms governing the development of convection and determining the precise location of precipitation systems. On the other hand, an ensemble approach appears absolutely necessary to take into consideration the uncertainty in the initial conditions and in the physics parameterizations for unresolved sub-grid scale processes (Yu and Tae-Young, 2010; Fiori et al., 2014; Miglietta et al., 2015).

The present study deals with an isolated heavy rain event, which was responsible for a flash flood in a very localized area in Calabria at the extreme southern tip of Italy. The rain persisted for about 2.5 hours (Chiaravalloti and Gabriele, 2009), during which the rainfall amount summed up to about 203 mm. Calabria, due to the presence of complex orography surrounded by a warm sea, is frequently affected by intense rainfall episodes. Seven cases with hourly rainfall larger than 50 mm h^{-1}, and three with rainfall accumulation larger than 200 mm h^{-1} in 24 h have been identified just during 2015 (data courtesy of IRPI-CNR).

Considering the importance of these events, which not only can significantly damage road and rail connections, but occasionally result in the loss of human lives, several episodes have been studied in the scientific literature. Generally, single case studies have been analysed (Federico and Bellecci, 2006; Federico et al., 2008a), also considering the sensitivity to upper level forcing (Federico et al., 2007) and the role of orography and sea surface fluxes (Federico et al., 2003). These studies pointed out that the peculiar geographical features of Calabria, i.e. the presence of steep mountain ranges near a warm sea, can lead to persistent precipitation patterns over localized areas. Federico et al. (2008b) found eleven circulation patterns associated with heavy rainfall in the region of Calabria, allowing the detection of the most recurrent circulation conducive to severe weather.

The paper is organized as follows. Section 2 describes the observations and synoptic conditions during the event. Section 3 introduces the numerical setup used for the present experiments. In Section 4, results are shown, focusing on both the sensitivity of the simulation to different setups and to the mechanisms responsible for the development of the rainfall; a discussion in terms of nondimensional parameters is also provided; conclusions are presented in Section 5.

2. Synoptic analysis and observations

As discussed above, the event of 3 July 2006 in Vibo Valentia (Calabria, Italy) was exceptional in intensity, and extremely localized since the most intense part affected an area of about 20 km^2 (Chiaravalloti and Gabriele, 2009). Apparently, no large-scale systems were present over the Italian peninsula; the Meteosat Second Generation (MSG) data (unfortunately no radar data and radiosoundings were available nearby) suggest the event can be classified as convective, as it will be shown in more detail in Section 2.1. Figure 1 shows the rain gauges available in the study area. The stations a few km away from Vibo recorded a maximum of only 8 mm during the whole event, clearly showing its very localized character. Thus, for its short duration and limited extent, the case study of 3 July 2006 represented a serious challenge for forecasters, both from the operational point of view and from the perspective of better understanding the mechanisms responsible for its genesis.

We start the analysis describing the synoptic conditions. The European Center for Medium-range Weather Forecast (ECMWF) analyses (Simmons, 1991) with 0.25° horizontal resolution are shown in Figure 2. In particular, the 500 hPa geopotential height and the mean sea level pressure (MSLP) at 1200 UTC 2 July (Figure 2a), thus before the event, and 1200 UTC 3 July (Figure 2b), after its occurrence, are shown.

The 500 hPa maps at 1200 UTC 2 July (Figure 2a) show an omega-like configuration, consisting of a ridge reaching the Scandinavian countries and two low pressure centers, one situated over the Atlantic coast of Portugal and the other one, weaker, centered over the Greek islands. Southern Italy is marginally affected by the latter low pressure system, responsible for a northwesterly flow at upper levels. The MSLP field of 2 July 1200 UTC (Figure 2a) shows, similarly, that also at lower levels southern Italy is affected by a northerly flow associated with the low pressure centered in the eastern Mediterranean area. At 1200 UTC 3 July (Figure 2b), the configuration at 500 hPa is very similar to 24 hour before, but showing an intensification of the low pressure center in the Mediterranean. We observe a similar situation also for the MSLP field (Figure 2b); however, the formation of a small low pressure minimum near the Tyrrhenian coast of southern Italy determines some variability in the surface winds within the prevailing northwesterly flow. This type of synoptic configuration has been classified by Federico et al. (2008a) as one of the favorable settings (cluster AP11) for convective development in Calabria. Looking at the 300 hPa maps (not shown) we can identify a straight jet stream near Calabria. Although Chiaravalloti and Gabriele (2009) showed that the maximum is located near the east (Ionian) coast of Calabria region at 1200 UTC, the simulations analysed here point out that during the development of the episode, the maximum wind was identified on the northern coast of Calabria, which may have favored the development and maintenance of convection.

2.1. *Satellite interpretation*

The severe storm was localized on few tens of squared kilometres inducing an exceptional and intense rainfall. Satellite images well describe the evolution of convection from the early morning around 0500 UTC until 1030 UTC when the rainrate reached the maximum value of 35 mm in 15 min (Chiaravalloti and Gabriele, 2009). The only two available NOAA satellite overpasses allow quantifying the rain rates by evaluating the cloud type with the 183-WSL (Laviola and Levizzani, 2011; Laviola et al., 2013) and MicroWave Cloud Classification (MWCC) method (Miglietta et al., 2013), respectively. In the early morning, a shallow convection producing precipitation intensity lower than 10 mm h^{-1} formed, partially saturating the soil. By using the rain gauge measurements reported in Chiaravalloti and Gabriele (2009) as ground truth, the persistence of convection over the Vibo Valentia area can also be shown by exploiting a sequence of MSG-SEVIRI images (Figure 3). The retrieval with the 183-WSL (Figure 4, left panel) combined with that of the MWCC for cloud classification (Figure 5, left panel) clearly demonstrate the weak intensity of convection at 0500 UTC. This conclusion is reinforced by the relatively high brightness temperatures at the top of clouds measured by MSG, with values around 240 K. The mature stage of convection, which corresponds to the maximum vertical development and the highest rain intensity, is depicted in the right panels of Figures 4 and 5, respectively. The quantification of rain rates, as assessed by 183-WSL, is around 15 mm h^{-1} when the convection is towering up to the top of the troposphere (8-10 km) with MSG cloud top temperatures of around 210 K.

3. Model setup and numerical experiments

A brief description of the model set up and the conditions of the experiments performed with the Weather Research and Forecasting (WRF) model version ARW-3.7.1 (Skamarock et al., 2008) is described here. WRF domains are shown in Figure 1. Three nested domains were defined in the "control run", following a one-way nesting strategy: the coarse-resolution domain designated as D01 (15-km grid spacing) covers the central Mediterranean basin, the intermediate domain D02 (3-km grid spacing) covers southern Italy and the inner most domain D03 (600-m grid spacing) covers approximately the Calabria region. In the three domains, 41 sigma levels are considered with the model top at a constant pressure surface (50 hPa). Sigma levels are not equally spaced, defining higher vertical resolution in the lower levels (10 sigma levels up to 900 hPa).

Different physics parameterization schemes are available in WRF for different processes. In the control run, we applied the Thompson scheme (Thompson et al., 2008) for microphysical processes, the Kain-Fritsch scheme (Kain, 2004) for convective parameterization, applied only to D01, the 5-layer Thermal Diffusion land surface scheme (Janjic, 1996) and MM5 Similarity surface layer scheme (Zhang and Anthes, 1982), the rapid radiative transfer (RRTM) model for longwave radiation (Mlawer et al., 1997), and the Dudhia scheme for shortwave radiation (Dudhia, 1989). Finally, the YSU PBL was used as boundary layer scheme (Hong and Dudhia, 2006). This combination of parameterizations has successfully been tested in the past in another case of intense convection in southern Italy (Miglietta and Regano, 2008).

The ECMWF analyses (Simmons, 1991) were used as initial and boundary conditions, the latter updated every 3 hours. Temporal resolution of the output was 3 h for D01 and D02 and 1 h for D03. The period covered by the simulation was 24 h, beginning at 1200 UTC on 2 July 2006. Other starting times have been tested but only the initial time corresponding to the best model results is analyzed hereafter.

4. Results

4.1. Sensitivity

Recently, Barrett et al. (2015) explored the possibility to simulate some convective rainbands in England with an ensemble approach, finding that while the topography provides some predictability, the simulation accuracy remains a forecast challenge. In order to explore this point also in our case study, we start considering the role of different large scale forcing on the model simulations.

Figure 6 shows the differences between the control simulation and a test simulation with initial and boundary conditions provided by the Final (FNL) Operational Global Analyzes from National Centers for Environmental Prediction (NCEP). Note that ECMWF analyses are the result of an operational daily routine and have a higher resolution (0.25° of grid spacing in 2006); in contrast, FNL are the final analysis from NCEP, where additional data are added a-posteriori to modify the operational real-time analysis. They have a coarser grid spacing of 1°. Figure 6a shows that the control run is able to correctly localize the rainfall peak. Although the hourly precipitation (not shown) is underestimated and anticipated by a few hours compared to the observations, the simulation is nevertheless able to reproduce a remarkable amount (80 mm), concentrated in a couple of hours as in the observations (Chiaravalloti and Gabriele, 2009). Also, the precipitation appears elongated in a rainband (a similar pattern can be identified from satellite) in the direction of the upper level flow. In contrast, the FNL test (Figure 6c) only simulates 45 mm and the location of maximum precipitation is shifted farther east of Vibo Valentia station. To understand the reasons for such differences, the 850 hPa geopotential height maps of the control run (Figure 6b) and FNL test (Figure 6d) are compared at 1200 UTC 2 July, i.e, the initial time of the simulation. Both maps show a very similar synoptic configuration, close to that described in Figure 2. However, the FNL analysis shows a positive bias with higher geopotential heights all over the domain. Also, over southern Italy the two analyses look slightly different, with a stronger pressure gradient in the ECMWF analysis while a cyclonic curvature is more apparent near Calabria in the FNL analysis. Finally, the 850 hPa temperature is very similar between the control run (Figure 6b) and FNL test (Figure 6d), with temperatures around 290 K in Calabria region. Apparently, small differences between the large-scale analyses were responsible for significant changes in the rainfall patterns.

In order to consider how a change in horizontal resolution could affect the rainfall amount, first we show in Figure 7a the rainfall simulated in D02 in the control run. Although the amount of precipitation simulated by the WRF model is similar to that in D03, the location of precipitation is not so accurate as in the latter domain due to its coarser horizontal resolution (the grid spacing in D02 is 3 km), which does not allow to represent sufficiently the orography of the region. Figure 7b shows the rainfall in an experiment with similar setup as the control run, and grid spacing of 1 km in the inner grid, 4 and 16 km respectively in the coarser domains, but domain size similar to the control run. In this case, the accumulated precipitation is greater (around 95 mm) compared to D03 in the control run, but, as in Figure 7a, the location of the maximum precipitation is farther east of Vibo Valentia station. Both tests highlight the importance of a fine horizontal resolution, particularly in the inner grid, to correctly represents the topography of the region and identify correctly the location of the convective rainfall.

Other simulation tests were performed to check the sensitivity of the model to different parameterization schemes (in particular, microphysics and PBL). For this purpose, experiments differing from the control run for the use of the Goddard (Tao et al., 1989) and WSM6 (Hong and Lim, 2006) microphysics, and for the MYNN2 (Nakanishi and Niino, 2006) and ACM2 (Pleim, 2007) PBL schemes were performed, modifying only one scheme at a time. Sensitivity experiments to PBL schemes, respectively using ACM2 (Figure 7c) and MYNN2 (Figure 7d), present similar precipitation amounts to the control run, with maxima between 75 and 85 mm, but the location of the precipitation peaks are placed again in the wrong position, northeastward of the Vibo Valentia gauge.

Finally, the tests with Goddard (Figure 7e) and WSM6 (Figure 7f) schemes produce an incorrect location of convection, shifted some tens of km to the east, and understimate the amount of precipitation significantly.

Summarizing, it turns out that the predictability of this case was extremely limited. Changing either the spatial resolution or the parameterization of the PBL may significantly affect the location of the heavy rainfall, although the simulated amount changed only slightly. In contrast, microphysical parameterizations can significantly influence also the rainfall amount. Taking into account that the period when most of the precipitation was recorded by the observations and simulated by the model were similar, the understimation in the cumulated precipitation is mainly due to a weaker rainfall intensity than to a lack of stationarity of the storm. In the following, only the results of the control run will be discussed.

4.2. Instability

Johns and Doswell III (1992) and Houze (1993) defined three general requirements for convective development: sufficiently deep instability layers, sufficient moisture at the lowest levels, and a triggering mechanism that activates the convective process if sufficient energy is available in the atmosphere. To study the first two conditions, thermodynamic indices are usually defined, which indicate potential storm development according to air mass properties such as humidity, temperature and helicity (Kunz, 2007). With this preamble, we are going to focus on the analysis of some parameters and instability indices related to instability and moisture.

The maximum precipitation detected by WRF in the control run, was simulated at 0600 UTC, with a rainfall rate of about 60 mm in one hour. Hereafter, we want to analyse whether environmental conditions conducive to convection were detected by the control run a few hours before the rainfall started. For this purpose, six instability indices have been analysed at 0300 UTC on July 3: most unstable CAPE (MCAPE) (Moncrieff and Miller, 1976), level of free convection (LFC), total totals (TT) (Miller, 1972) and potential instability (PI) (Saucier, 1955), most unstable convective inhibition (MCIN) (Colby, 1984) and mean relative humidity in the lower 300 hPa (MRH) indices. MCAPE and MCIN were calculated using the most unstable lifted parcel, i.e. the parcel with maximum equivalent potential temperature (θe) in the column.

Figure 8a shows that very high values of MCAPE (up to 3000 Jkg^{-1}) affect the southern Tyrrhenian Sea, i.e. the region upstream of Vibo Valentia. This area of high instability reaches the interior of Calabria, indicating high energy availability in the first hours of July 3, just before the episode. At the same time, LFC (Figure 8b) is low, between 400 and 600 m, in the same region. Thus, in the presence of a small uplift, strong convective activity may easily develop.

To further analyse the instability and the moisture present in the area in pre-convective conditions, Figure 9 shows four other instability indices. Figure 9a shows the TT index: values around 50 K are simulated in a band extending from west-northwest to east-southeast from the Tyrrhenian to the Ionian Sea, reaching its maximum of 54 K in the interior of Calabria: such values are generally indicative of possible severe thunderstorms. Figure 9b shows that the pattern of PI (defined as the difference between θe at 500 hPa and at 850 hPa) is very similar to that of TT, with negative values down to -20 K, indicating the presence of great instability in that area. This is mainly due to very high values of θe at low levels in the Tyrrhenian Sea, combined with low values of θe in the upper level (around 500 hPa) over the Ionian Sea but extending toward the northern part of Calabria region, with a minimum value of 322 K at 400 hPa (not shown). Figure 9c shows that the high θe at low levels is mainly due to the high moisture content, since large areas in Calabria show averaged relative humidity above 80% in the lower 3 km. Such high moisture content is responsible for very small values of MCIN (Figure 9d) simulated over the Tyrrhenian Sea and in the interior of Calabria.

The band of high low-level moisture content, which is responsible for the high values of all the instability indices, is shown in Figure 9 and is advected by the prevailing northwesterly flow, associated with the small low pressure minimum near the Tyrrhenian coast of southern Italy, from the central Tyrrhenian sea southeastward. This is shown more clearly in Figure 10.

Figures 10a and 10b show cross-sections (from NW to SE) of θe and the water vapor mixing ratio 12 hours and 6 hours before the precipitation peak, respectively, in D02. At 1800 UTC (Figure 10a), high values of θe up to 348 K are observed between the horizontal grid points 0 and 60, over the Tyrrhenian Sea, while in the northern part of the mountain, θe does not reach 340 K. In contrast, 6 hours later (Figure 10b), the area with high water vapor content is horizontally advected toward the mountain, increasing the low level θe and creating an unstable environment near Vibo.

The motivation for such a high moisture content can be understood analyzing sea surface temperature (SST) field. Many authors have studied the role of the SST and latent heat flux (LHT) in convection development in extratropical areas (M.Beljaars, 1995; Bretherton et al., 2005; Yokoi et al., 2014) and more specifically in the Mediterranean (Khain et al. (1993); Miglietta et al. (2011); Cassola et al. (2016). The Italian National Research Council (CNR) has recently produced daily (nighttime), 4 km resolution REP L4 MED datasets (Pisano et al., 2016), based on the latest Pathfinder v5.2 AVHRR dataset (1982-2012, Casey et al. (2010), and freely distributed through the CMEMS. Figure 11a, which represents the SST on July 3, shows very high temperatures up to 301 K (red areas), covering all the southern Tyrrhenian Sea. Also, an intense LHT (Figure 11b) up to 400 Wm^{-2} is found, mainly as a consequence of the intense low-level flow across the area indicating a strong energy transfer from the sea to the atmosphere. These fluxes have the effect of increasing the humidity and the temperature in the lower levels, determining conditions closer to saturation and increasing θe in the lower troposphere, and consequently PI. Incidentally, as a consequence of the low level wind structure, the fluxes are particularly strong in a filament elongated from the Tyrrhenian Sea up to the coast near Vibo Valentia (Figure 11b). On the other hand, another area with high values of LHT is present in the Ionian Sea; however, the properties of the air mass in this area are different, since it is characterized by low moisture in the low-middle troposphere and lower MCAPE, thus conditions unfavorable for the development of convection.

4.3. Mechanisms of convection

To analyse further the triggering mechanisms involved in convection, θe and the cloud water plus ice content at 0300 UTC (Figure 12b), 0500 UTC (Figure 12c) and 0600 UTC (Figure 12d) on 3 July are plotted along a NNW-SSE cross section (thus along the prevailing wind direction and the precipitation line) whose position is shown in Figure 12a. The cross-section extends vertically from 1000 to 250 hPa and represents model fields in D03. Figure 12b shows a perturbation in θe, associated with potentially warm air in the middle troposphere, a few km upstream of the coastline (at point x = 30). The isotherms are very dense between 750 and 650 hPa, producing an increase in the (negative) vertical gradient of θe, locally determining conditions of enhanced instability.

Figures 12c and 12d present the cross-section when the onset of convection was detected (at 0500 UTC) and at the time of maximum intensity (at 0600 UTC), respectively. At the beginning of convection (Figure 12c), the disturbance observed at 0300 UTC reaches the orography of the region, which provides the uplift necessary for releasing the instability. Apparently, the uplift due to the small bump (a few hundred meters high) near Vibo, located upstream of the Apennines (which are farther east in the cross section) is sufficient to overcome the inhibition. As a consequence, convective cells develop, from the boundary layer up to 400 hPa. The maximum water and ice content is found at low levels (around 800 hPa), reaching a value of 1.6 g kg^{-1}. Figure 12d shows that one hour later convection develops downstream of the first obstacle, closer to the main mountain range. At this time, the vertical extent of the cloud reaches again 400 hPa; however, in contrast to the previous time, the highest amounts of water and ice content (up to 2.4 g kg^{-1}) are found in the highest levels. This increase of cloud content at high levels is consistent with the increase of vertical velocities during the convective development, especially at 0600 UTC when a maximum speed of 16 m s^{-1} was detected (not shown).

The present analysis has shown that, within an environment favorable to convection, the advection of a θe perturbation may have locally enhanced the instability, which is released when the airflow impinges on the mountain. It remains to be determined whether low-level mechanisms may have also contributed to the exact localization of rainfall. Low-level convergence upstream of the mountain and over the sea is a frequent lifting mechanism induced by the alteration of the low-level flow by mountains and islands, which is particularly effective in the Mediterranean (Duffourg et al., 2016). In fact, mountainous terrain can influence atmospheric flow in the mesoscale through lifting, flow deviation or blocking with a strong impact on the development of precipitating convection (Barthlott et al., 2014). Calabria has a complex orography that can generate and deviate local winds to determine areas of low level convergence. In a region surrounded by the sea as Calabria, on a local scale sea (and land) breezes driven by differential heating can also contribute to convergence patterns leading to convection initiation. Figure 13 shows a detail of the area affected by the peak of precipitation (box in Figure 12a), where the water vapor flux divergence, wind vectors at 925 hPa and the 24-h accumulated precipitation (from 2 July at 1200 to 3 July at 1200) are represented. It is remarkable that the maximum water vapor flux convergence is co-located with the precipitation maximum over a relatively low but very steep orograpic peak around 500 m high, which is separated from a higher orographic obstacle by a narrow valley. The peculiar small-scale orographic features appear to favor convergence in two points, respectively located above the small peak (corresponding to the precipitation maximum) and a few km farther downstream, determining the rainband pattern present in the simulations.

Numerical studies have shown the role of small-scale topographic obstacles in triggering and anchoring the rainfall (Kirshbaum and Durran, 2005a,b). This is true particularly in subtropical humid climate zones, where the lower atmosphere is very humid and the LFC is often very low, so that convection can easily occur even for a small vertical lifting (Umemoto et al., 2004). The Mediterranean sea can also show similar conditions. For example, Miglietta and Regano (2008) showed that the low Murge hills in Apulia (about 700 m high) were able to trigger convection in a moist conditionally unstable flow from the Ionian Sea, producing a flash flood in southeastern Italy.

4.4. Nondimensional analysis

Analysis of the vertical profiles simulated by WRF model 30 km upstream of the rainfall peak identified by the model, can give a better idea of the changing environmental conditions before the start of rainfall. Figure 14 shows the simulated soundings at 1800 UTC 2 July (Figure 14a), at 0000 UTC (Figure 14b) and at 0300 UTC 3 July (Figure 14c). Figure 14a shows that the environmental conditions initially are far from saturation. The wind field, predominantly northwesterly, shows weak vertical shear both in terms of direction and intensity throughout the profile. In Figures 14b, the atmosphere is saturated from low levels to a height of 800 hPa, which is consistent with the very moist air observed in Figure 9c and Figure 10b. Nearly saturated conditions persist in the low levels also at 0300 UTC (Figure 14c). It is interesting to note that the low-level wind changes to southwesterly at 0000 UTC (Figure 14b), becoming westerly at 0300 UTC (Figure 14c) while the wind speed slightly intensifies. Such modifications may affect the interaction of the flow with the orography by modifying the component of the wind perpendicular to the obstacle.

The orographic mechanism responsible for the uplift and the intensification of convection may be analysed using some nondimensional parameters. These fields are evaluated in the same place as the vertical profiles, 30 km upstream of the rainfall peak, thus not directly affected by the interaction of the flow with the orography and the eventual development of orographic convection. Their values are reported in Table 1, showing also the time evolution before, during and after the storm occurrence.

First, we consider the Froude number (Fr), which allows to roughly estimate whether the wind is able to flow over or around the orographic obstacle (Smith, 1979; Miglietta and Buzzi, 2004). In the present study, it is defined as: $Fr = hN/U$, where $h = 450$ m is the approximate mountain height of the hill near Vibo the atmospheric flow impinges on, N the moist Brunt-Väisälä frequency (in the lower 1 km, and U the wind speed averaged in the lower 1 km), which is the depth of the layer more directly affected by the interaction of the flow with the orography. Although it may be questionable to use Fr for the identification of the flow regime in the case of moist conditionally unstable flows, we believe that its time variation can provide some useful information about the transition between the two regimes of flow over and flow around (Davolio et al., 2016).

As a consequence of the intensification of the low level flow immediately before the event, Fr increases above 1: this value represents conditions favorable to "flow over" the obstacle. Thus, the air impinging over the mountain can be easily lifted and reach the level of free convection, which is low in the present case (h/LFC, defined following Miglietta and Rotunno (2009), is about 0.7 at 0300 UTC, thus LFC is around 600 m), as also discussed in Subsection 4.1. On the other hand, the conditions appear less favorable both before and after the simulated event, due to the higher value of LFC.

Miglietta and Rotunno (2009, 2010) identified some non-dimensional numbers, depending on the mountain geometry and the dynamic and thermodynamic characteristics of the airflow, to evaluate the typology of solution one should expect in the case of conditionally unstable flows past a mesoscale mountain ridge. The parameter that better identifies the behavior of the solution in moist conditionally unstable conditions is (see Fig. 1 in Miglietta and Rotunno (2012)) the rate of the advective time scale a/U to the convective time scale $h_{trop}/(CAPE)^{0.5}$, where h_{trop} is the height of the tropopause. In the present case, it is about 5 during the event, suggesting the presence of conditions favorable to stationary orographic convection (Fig. 3a in (Miglietta and Rotunno, 2010). Effectively, in the present case study, the orographic rainfall appears persistent in the same area during the whole duration of the event. This fact, combined with the analysis of the temperature field in the low levels, excludes the presence of cold pools induced by the evaporation of rainfall.

5. Conclusions

A heavy rainfall convective event in the Calabria region (southern Italy) with a recorded precipitation amount of more than 200 mm in 2.5 h, and affecting an area of about 20 km^2, has been analysed. This case study, based on high-resolution WRF model simulations validated by raingauge observations, presents a high degree of complexity due to its very localized occurrence and the complexity of the responsible mechanisms. Considering the peculiar morphology of the region, several mechanisms could be responsible for the localized triggering of convection, for example, lee waves induced by small-scale obstacles (as in Kirshbaum et al. (2007b,a)), mountain thermal circulation over the local mountains, sea-breeze convergence due to the convex coastline in the region, or a combination of mountain and sea-breeze circulation. Looking at the model simulation, none of these mechanisms appear effective in the present case. In contrast, the rainfall appears to be generated by a combination of other factors: an environment extremely favorable to convection determined by MCAPE values greater than 3000 J kg^{-1} and TT values around 54 K, associated with high moisture content in the low levels, which determines high potential instability, low LFC and small MCIN; the presence of a small perturbation in θe that temporarily and locally enhances the instability; the lifting induced by the orography, which removes the small inhibition allowing their air parcels to reach the level of free convection.

The exact localization of the rainfall event is associated with the low-level convergence induced by the peculiar morphology of the region, which deflects the low-level flow determining the development of convection near Vibo.

Moreover, the sensitivity experiments show the importance of PBL and microphysics parametrization schemes for the correct prediction of precipitation both in the amount and localization. An ensemble approach using advanced data assimilation methods appears necessary to account for the limitations in the representation of the initial conditions and in the model formulation especially in events like this, showing strong sensitivity to different numerical setups. Additional tests highlight the importance of defining grids (in particular the inner one) with fine horizontal resolution. This allows to represent correctly the topography of the region, thus allows for a more correct localization of the convective rainfall. About this point, other heavy rain events have been recorded in recent years near Vibo Valentia, suggesting the importance of the small scale orography to determine their localization in the same area. This peculiar morphology determines a stationary triggering location, just upstream of Vibo Valentia. The rainfall event appears due to individual convective cells, although the repeated initiation of cells at a fixed location and their advection downstream gave them a banded appearance.

The present study identifies a peculiar mechanism that may play an important role in other heavy rain events in the region and in other areas with similar characteristics. The analysis of additional events will possibly give a better understanding of this type of event in the Mediterranean area and provide a more robust statistical support to these results.

Acknowledgments

The present work develops in the framework of RAMSES project funded by Rete Ferroviaria Italiana. The stay of Estibaliz Gascon at ISAC-CNR is supported by METEORISK PROJECT (RTC-2014-1872-5). The authors thank Dr. Richard Rotunno and Dr. Guglielmo Lacorata for having carefully read the manuscript and for relevant suggestions. Thanks also to Andrea Pisano and the GOS group of ISAC-CNR for providing SST data.

References

Altinbilek, D., Barret, E.C., Oweis, T., Salameh, E., Siccardi, F., 1997. Rainfall climatology on the Mediterranean, EU-AVI 080 Project ACROSS-analyzed climatology rainfall obtained from satellite and surface data in the Mediterranean basin. EC reports .

Barrett, A.I., Gray, S.L., Kirshbaum, D.J., Roberts, N.M., Schultz, D.M., Fairman, J.G., 2015. Synoptic versus orographic control on stationary convective banding. Q. J. R. Meteorol. Soc. 141, 1101–1113. doi:10.1002/qj.2409.

Barthlott, C., Adler, B., Kalthoff, N., Handwerker, J., Kohler, M., Wieser, A., 2014. The role of Corsica in initiating nocturnal offshore convection. Q. J. R. Meteorol. Soc. doi:10.1002/qj.2415.

Bretherton, C.S., Blossey, P.N., Khairoutdinov, M., 2005. An energy-balance analysis of deep convective self-aggregation above uniform SST. J. Atmos. Sci. 62, 4273–4292. doi:10.1175/JAS3614.1.

Casey, K.S., Brandon, T.B., Cornillon, P., Evans, R., 2010. The past, present, and future of the AVHRR pathfinder SST program. Oceanography from Space: Revisited. pp. 273–287. doi:10.1007/978-90-481-8681-5_16.

Cassola, F., Ferrari, F., Mazzino, A., Miglietta, M.M., 2016. The role of the sea on the flash floods events over Liguria (northwestern Italy). Geophys. Res. Lett. 43, 3534–3542. doi:10.1002/2016GL068265.

Chappell, C.F., 1986. Quasi-stationary convective events. Mesoscale Meteorology and Forecasting. (P.S. Ray, Ed.). Amer. Meteor. Soc. pp. 289–310.

Chiaravalloti, F., Gabriele, S., 2009. Vibo Valentia flood and MSG rainfall evaluation. Atmos. Res. 93, 286–294.

Colby, J.F.P., 1984. Convective inhibition as a predictor of convection during AVE-SESAME II. Mon. Weather Rev. 112, 2239–2252.

Davis, C.A., Lee, W.C., 2012. Mesoscale analysis of heavy rainfall episodes from SoWMEX/TiMREX. J. Atmos. Sci. 69, 521–537. doi:10.1175/JAS-D-11-0120.1.

Davolio, S., Volonté, A., Manzato, A., Pucillo, A., Cicogna, A., Ferrario, M.E., 2016. Mechanisms producing different precipitation patterns over north-eastern Italy: insights from HyMeX-SOP1 and previous events. Q. J. R. Meteorol. Soc. doi:10.1002/qj.2731.

Delrieu, G., Nicol, J., Yates, E., Kirstetter, P., Creutin, J., Anquetin, S., Obled, C., Saulnier, G., Ducrocq, V., Gaume, E., et al., 2005. The catastrophic flash-flood event of 8-9 September 2002 in the Gard region, France: A first case study for the Cevennes-Vivarais Mediterranean Hydrometeorological Observatory. J. Hydrometeorol. 6, 34–52.

Ducrocq, V., Braud, I., Davolio, S., Ferretti, R., Flamant, C., Jansa, A., Kalthoff, N., Richard, E., Taupier-Letage, I., Ayral, P.A., Belamari, S., Berne, A., Borga, M., Boudevillain, B., Bock, O., Boichard, J.L., Bouin, M.N., Bousquet, O., Bouvier, C., Chiggiato, J., Cimini, D., Corsmeier, U., Coppola, L., Cocquerez, P., Defer, E., Delanoë, J., Di Girolamo, P., Doerenbecher, A., Drobinski, P., Dufournet, Y., Fourrié, N., Gourley, J., Labatut, L., Lambert, D., Le Coz, J., Marzano, F., Molinié, G., Montani, A., Nord, G., Nuret, M., Ramage, K., Rison, W., Roussot, O., Said, F., Schwarzenboeck, A., Testor, P., Van Baelen, J., Vincendon, B., Aran, M., Tamayo, J., 2014. HyMeX-SOP1: The Field Campaign Dedicated to Heavy Precipitation and Flash Flooding in the Northwestern Mediterranean. Bull. Amer. Meteor. Soc. 95, 1083–1100.

Dudhia, J., 1989. Numerical study of convection observed during the Winter Monsoon Experiment using a mesoscale two-dimensional model. J. Atmos. Sci. 46, 3077–3107.

Duffourg, F., Nuissier, O., Ducrocq, V., Flamant, C., Chazette, P., Delanoë, J., Doerenbecher, A., Fourrié, N., Di Girolamo, P., Lac, C., Legain, D., Martinet, M., Saïd, F., Bock, O., 2016. Offshore deep convection initiation and maintenance during the HyMeX IOP 16[a] heavy precipitation event. Q. J. R. Meteorol. Soc. doi:10.1002/qj.2725.

Federico, S., Avolio, E., Bellecci, C., Lavagnini, A., Colacino, M., Walko, R.L., 2008a. Numerical analysis of an intense rainstorm occurred in southern Italy. Nat. Hazards Earth Syst. Sci. 8, 19–35. doi:10.5194/nhess-8-19-2008.

Federico, S., Avolio, E., Bellecci, C., Lavagnini, A., Walko, R.L., 2007. Predictability of intense rain storms in the Central Mediterranean basin: sensitivity to upper-level forcing. Adv. in Geosciences 12, 5–18.

Federico, S., Avolio, E., Pasqualoni, L., Bellecci, C., 2008b. Atmospheric patterns for heavy rain events in Calabria. Nat. Hazards Earth Syst. Sci. 8, 1173–1186. doi:10.5194/nhess-8-1173-2008.

Federico, S., Bellecci, C., 2006. The 11-12 December 2003 storm in Southern Italy. Adv. in Geosciences 7, 37–44.

Federico, S., Bellecci, C., Colacino, M., 2003. Quantitative precipitation of the Soverato flood: the role of orography and surface fluxes. Il Nuovo Cimento 26 C, 7–22.

Fiori, E., Comellas, A., Molini, L., Rebora, N., Siccardi, F., Gochis, D.J., Tanelli, S., Parodi, A., 2014. Analysis and hindcast simulations of an extreme rainfall event in the Mediterranean area: The Genoa 2011 case. Atmos. Res. 138, 13–29.

Gheusi, F., Stein, J., 2003. Small-scale rainfall mechanisms for an idealized convective southerly flow over the Alps. Q. J. R. Meterol. Soc. 129, 1819–1840.

Hong, S.Y., Dudhia, J., 2006. A new vertical diffusion package with an explicit treatment of entrainment processes. Mon. Wea. Rev. 134, 2318–2341.

Hong, S.Y., Lim, J.O.J., 2006. The WRF single-moment 6-class microphysics scheme (WSM6). J. Korean Meteor. Soc. 42, 129–151.

Houze, R.A., 1993. Cloud dynamics. Academic press.

Janjic, Z.I., 1996. A Multi-layer Soil Temperature Model for MM5, in: The sixth PSU/NCAR MM5 Users' Workshop, Boulder, Colorado. pp. 49–50.

Johns, R.H., Doswell III, C.A., 1992. Severe local storms forecasting. Weather Forecast. 7, 588–612.

Kain, J.S., 2004. The Kain-Fritsch convective parameterization: An update. J. Appl. Meteor. 43, 170–181.

Khain, A.P., Rosenveld, D., Sednev, I., 1993. Coastal effects in the Eastern Mediterranean as seen from experiments using a cloud ensemble model with detailed description of warm and ice microphysical processes. Atmos. Res. 30, 295–319. doi:10.1016/0169-8095(93)90029-N.

Kirshbaum, D.J., Bryan, G.H., Rotunno, R., Durran, D.R., 2007a. The triggering of orographic rainbands by small-scale topography. J. Atmos. Sci. 64, 1530–1549. doi:10.1175/JAS3924.1.

Kirshbaum, D.J., Durran, D.R., 2005a. Factors governing cellular convection in orographic precipitation. J. Atmos. Sci. 62, 3758–3774.

Kirshbaum, D.J., Durran, D.R., 2005b. Observations and modeling of banded orographic convection. J. Atmos. Sci. 62, 1463–1479.

Kirshbaum, D.J., Rotunno, R., Bryan, G.H., 2007b. The spacing of orographic rainbands triggered by small-scale topography. J. Atmos. Sci. 64, 4222–4245. doi:10.1175/2007JAS2335.1.

Kunz, M., 2007. The skill of convective parameters and indices to predict isolated and severe thunderstorms. Nat. Hazards Earth Syst. Sci 7, 327–342.

Laviola, S., Levizzani, V., 2011. The 183-WSL fast rain rate retrieval algorithm. Part I: Retrieval design. Atmos. Res. 99, 443–461. doi:10.1016/j.atmosres.2010.11.013.

Laviola, S., Levizzani, V., Cattani, E., Kidd, C., 2013. The 183-WSL fast rain rate retrieval algorithm. Part II: Validation using ground radar measurements. Atmos. Res. 134, 77–86. doi:10.1016/j.atmosres.2013.07.013.

Llasat, M.C., Marcos, R., Turco, M., Gilabert, J., Llasat-Botija, M., 2016. Trends in flash flood events versus convective precipitation in the Mediterranean region: The case of Catalonia. J. Hydrol. .

Llasat-Botija, M., Llasat, M.C., López, L., 2007. Natural hazards and the press in the western Mediterranean region. Adv. Geosci. 12, 81–85.

M.Beljaars, A.C., 1995. The parametrization of surface fluxes in large-scale models under free convection. Q. J. R. Meteorol. Soc. 121, 255–270. doi:10.1002/qj.49712152203.

Miglietta, M.M., Buzzi, A., 2004. A numerical study of moist stratified flow regimes over isolated topography. Q. J. R. Meteorol. Soc. 130, 1749–1770. doi:10.1256/qj.02.225.

Miglietta, M.M., Laviola, S., Malvaldi, A., Conte, D., Levizzani, V., Price, C., 2013. Analysis of tropical-like cyclones over the Mediterranean sea through a combined modeling and satellite approach. Geophys. Res. Lett. 40, 2400–2405. doi:doi:10.1002/grl.50432,2013.

Miglietta, M.M., Mastrangelo, D., Conte, D., 2015. Influence of physics parameterization schemes on the simulation of a tropical-like cyclone in the Mediterranean Sea. Atmos. Res. 153, 360–375. doi:10.1016/j.atmosres.2014.09.008.

Miglietta, M.M., Moscatello, A., Conte, D., Mannarini, G., Lacorata, G., Rotunno, R., 2011. Numerical analysis of a Mediterranean "hurricane" over south-eastern Italy: Sensitivity experiments to sea surface temperature. Atmos. Res. 101, 412–426. doi:10.1016/j.atmosres.2011.04.006.

Miglietta, M.M., Regano, A., 2008. An observational and numerical study of a flash-flood event over south-eastern Italy. Nat. Hazards Earth Syst. Sci. 8, 1417–1430.

Miglietta, M.M., Rotunno, R., 2009. Numerical simulations of conditionally unstable flows over a mountain ridge. J. Atmos. Sci. 66, 1865–1885. doi:10.1175/2009JAS2902.1.

Miglietta, M.M., Rotunno, R., 2010. Numerical simulations of low-CAPE flows over a mountain ridge. J. Atmos. Sci. 67, 2391–2401. doi:10.1175/2010JAS3378.1.

Miglietta, M.M., Rotunno, R., 2012. Application of theory to observed cases of orographically forced convective rainfall. Mon. Wea. Rev. 140, 3039–3053. doi:10.1175/MWR-D-11-00253.1.

Miller, R.C., 1972. Notes on analysis and severe storm forecasting procedures of the Air Force Global Weather Center. Tech. Rep. 200 (Rev.), AWS, U.S. Air Force. 102 pp. Headquarters, Scott AFB, IL 62225.

Mlawer, E.J., Taubmana, S.J., Brown, P.D., Iacono, M.J., , Clough, S.A., 1997. Radiative transfer for inhomogeneous atmospheres: RRTM, a validated correlated-k model for the longwave. J. Geophys. Res. 102, 16663–16682.

Moncrieff, M., Miller, M., 1976. The dynamics and simulation of tropical cumulonimbus and squall lines. Q. J. R. Meteorol. Soc 102, 373–394.

Nakanishi, M., Niino, N., 2006. An improved Mellor-Yamada level 3 model: its numerical stability and application to a regional prediction of advecting fog. Bound. Layer Meteor. 119, 397–407.

Pisano, A., Nardelli, B.B., Tronconi, C., Santoleri, R., 2016. The new Mediterranean optimally interpolated pathfinder AVHRR SST Dataset (1982-2012). Remote Sens. Environ. 176, 107–16.

Pleim, J.E., 2007. A Combined Local and Nonlocal Closure Model for the Atmospheric Boundary Layer. Part I: Model Description and Testing. J. Appl. Meteor. Climatol. 46, 1383–1395.

Pontrelli, M.D., Bryan, G.H., Fritsch, J.M., 1999. The Madison County, Virginia, flash flood of 27 June 1995. Weather Forecast. 14, 384–404.

Rotunno, R., Houze, R.A., 2007. Lessons on orographic precipitation from the Mesoscale Alpine Programme. Q. J. R. Meteorol. Soc. 133, 811–830. doi:10.1002/qj.67.

Saucier, W.J., 1955. Principles of Meteorological Analysis. pp. 76–78.

Simmons, A.J., 1991. Development of a high resolution, semi-Lagrangian version of the ECMWF forecast model. Numerical Methods in Atmospheric Models. European Centre for Medium-Range Weather Forecasts Vol. 2, 281–324.

Skamarock, W.C., Klemp, J.B., Dudhia, J., Gill, D.O., Barker, D.M., Wang, W., Powers, J.G., 2008. A description of the Advanced Research WRF version 3. NCAR Tech. Note NCAR/TN-475+STR.

Smith, R.B., 1979. The influence of mountains on the atmosphere. Adv. Geophys. 21, 87–230.

Tao, W.K., Simpson, J., McCumber, M., 1989. An Ice-Water Saturation Adjustment. Mon. Wea. Rev. 117, 231–235.

Thompson, G., Field, P.R., Rasmussen, R.M., Hall, W.D., 2008. Explicit forecasts of winter precipitation using an improved bulk microphysics scheme. Part II: Implementation of a new snow parameterization. Mon. Weather Rev. 136, 5095–5115. doi:10.1175/2008MWR2387.1.

Umemoto, Y., Teshiba, M., Shibagaki, Y., Hashiguchi, H., Yamanaka, M.D., Fukao, S., 2004. Combined wind profiler-weather radar observations of orographic rainband around Kyushu, Japan in the Baiu season. Ann. Geophys. 22, 3971–3982.

Wulfmeyer, V., Behrendt, A., Kottmeier, C., Corsmeier, U., Barthlott, C., Craig, G.C., Hagen, M., Althausen, D., Aoshima, F., Arpagaus, M., Bauer, H., Bennett, L., Blyth, A., Brandau, C., Champollion, C., Crewell, S., Dick, G., Di Girolamo, P., Dorninger, M., Dufournet, Y., Eigenmann, R., Engelmann, R., Flamant, C., Foken, T., Gorgas, T., Grzeschik, M., Handwerker, J., Hauck, C., Höller, H., Junkermann, W., Kalthoff, N., Kiemle, C., Klink, S., König, M., Krauss, L., Long, C.N., Madonna, F., Mobbs, S., Neininger, B., Pal, S., Peters, G., Pigeon, G., Richard, E., Rotach, M.W., Russchenberg, H., Schwitalla, T., Smith, V., Steinacker, R., Trentmann, J., Turner, D.D., van Baelen, J., Vogt, S., Volkert, H., Weckwerth, T., Wernli, H., Wieser, A., Wirth, M., 2011. The Convective and Orographically-induced Precipitation Study (COPS): The scientific strategy, the field phase, and research highlights. Q. J. R. Meteorol. Soc. 137, 3–30. doi:10.1002/qj.752.

Yokoi, S., Katsumata, M., Yoneyama, K., 2014. Variability in surface meteorology and air-sea fluxes due to cumulus convective systems observed during CINDY/DYNAMO. J. Geophys. Res. Atmos. 119, 2064–2078. doi:10.1002/2013JD020621.

Yu, X., Tae-Young, L., 2010. Role of convective parameterization in simulations of a convection band at grey-zone resolutions. Tellus A 62, 617–632.

Zhang, D.L., Anthes, R.A., 1982. A high-resolution model of the planetary boundary layer sensitivity tests and comparisons with SESAME-79 data. J. Appl. Meteor. 21, 1594–1609.

Figure captions

Fig 1. External model domain (D01) and inner domains D02 and D03 defined for WRF model control run (left). Rain gauge network of the Civil Protection of Calabria near Vibo Valentia with 24 h accumulated precipitation (from 2 July at 1200 to 3 July at 1200) on 3 July (right).

Fig 2. ECMWF analysis of mean sea level pressure (hPa, solid contours) and 500 hPa geopotential height with contours every 40 gpm (m, filled contours) at 1200 UTC 2 July (a) and 1200 UTC 3 July (b).

Fig 3. The sequence of 30-minutes MSG brightness temperature at 10.8 μm shows the persistence of convection over Vibo Valentia. The time sequence fits the rain gauge measurements in Chiaravalloti and Gabriele (2009, Fig. 2).

Fig 4. Rain rate retrieval on 3 July 2006 using the 183-WSL method (zoomed in the red square near Vibo). The early morning convection (left panel, 0452 UTC) produces rainfall intensities lower than 10 mm h^{-1}. The intensification of the storm (right panel, 1018 UTC) producing the flooding is responsible for rainfall rates around 15 mm h^{-1}.

Fig 5. As in Figure 3 but for MSG-SEVIRI channel at 10.8 μm - 0500 UTC (left) and 1030 UTC (right), respectively -. The intensification of convection is described by the MSG brightness temperature values (240 K at 0500 UTC and 210 K at 1030 UTC) and by the MicroWave Cloud Classification (MWCC) method (red square). Legend: ST = Stratiform clouds; CO = Convective clouds; LHS = Large HailStones; XLHS = eXtra Large HailStones; SNF = SNowFall. Both for ST and CO, the category (1, 2, 3) increases with the cloud top altitude. From early morning, the convective system evolves from shallow convection (green and yellow colors) to deep convection (red colour) surrounded by stratiform clouds (blue and cyan).

Fig 6. 24 h accumulated precipitation (from 2 July at 1200 to 3 July at 1200) in WRF model, using ECMWF analysis (a) and FNL analysis (c) as initial conditions. 850 hPa temperature (K, solid contours) and geopotential height with contours every 20 gpm (m, filled contours) at 1200 UTC 2 July using ECMWF analysis (b) and FNL analysis (d). The brown point in a) and c) represents the position of Vibo Valentia rain gauge.

Fig 7. 24 h accumulated precipitation (from 2 July at 1200 to 3 July at 1200) in test runs having: D02 with 3 km horizontal resolution (a), D03 with 1 km horizontal resolution (b), ACM2 PBL scheme (c), MYNN2 PBL scheme (d), Goddard microphysicss scheme (e) and WSM6 microphysics scheme (f). The brown point represents the position of Vibo Valentia rain gauge.

Fig 8. Most unstable CAPE (MCAPE) (in J kg^{-1}, colors) (a) and level of free convection (LFC) (in m, colors) (b) at 0300 UTC 3 July.

Fig 9. Total totals index (TT) (a), potential instability (PI, in K), mean relative humidity in the lower 300 hPa (MRH, in %) (c) and Most unstable CIN (MCIN, in J kg^{-1}) (d) at 0300 UTC 3 July.

Fig 10. Equivalent potential temperature (θe) (black lines, c.i.= 4 K), and water vapor mixing ratio (colors, c.i.= 2 g kg^{-1}) are shown along a NW-SE cross section in D02 (cross-section line drawn in the upper left corner of the figures) at 1800 UTC 2 July (a) and 0000 UTC 3 July (b) 2006.

Fig 11. Observed daily averaged sea surface temperature (SST, in K) on 3 July (a) and simulated latent heat flux (LHT, in W m^{-2}) at 0300 UTC 3 July (b).

Fig 12. a) Location of cross-section and 24 h accumulated precipitation (from 2 July at 1200 to 3 July at 1200) in D03. The brown frame corresponds to the area represented in Figure 13. The brown point represents the position of the Vibo Valentia rain gauge (a); equivalent potential temperature (θe) (black lines, c.i.= 3 K), and cloud water plus ice content (colors, c.i.= 0.2 g kg^{-1}) are shown along a NW-SE cross section at 0300 UTC (b), 0500 UTC (c) and 0600 UTC (d) 3 July 2006.

Fig 13. Terrain height (black lines, at 100 m interval), water vapor flux divergence (colors, g m^{-2} s^{-1}) and 925 hPa wind arrows (m s^{-1}) at 0500 UTC 3 July; 24-h accumulated precipitation, from 2 July at 1200 to 3 July at 1200(black bolded lines, at 20 mm interval). The brown line denotes the coastline.

Fig 14. Skew-T diagrams computed from WRF in a location 30 km upstream of the simulated rainfall peak (dewpoint data: blue line, temperature data: red line) at 1800 UTC 2 July (a), 0000 UTC (b) and 0300 UTC (c) 3 July 2006.

Table 1. Table with some instability parameters, calculated 30 km upstream the simulated rainfall peak from 1800 UTC 2 July to 12 UTC 3 July at 3-hours intervals.

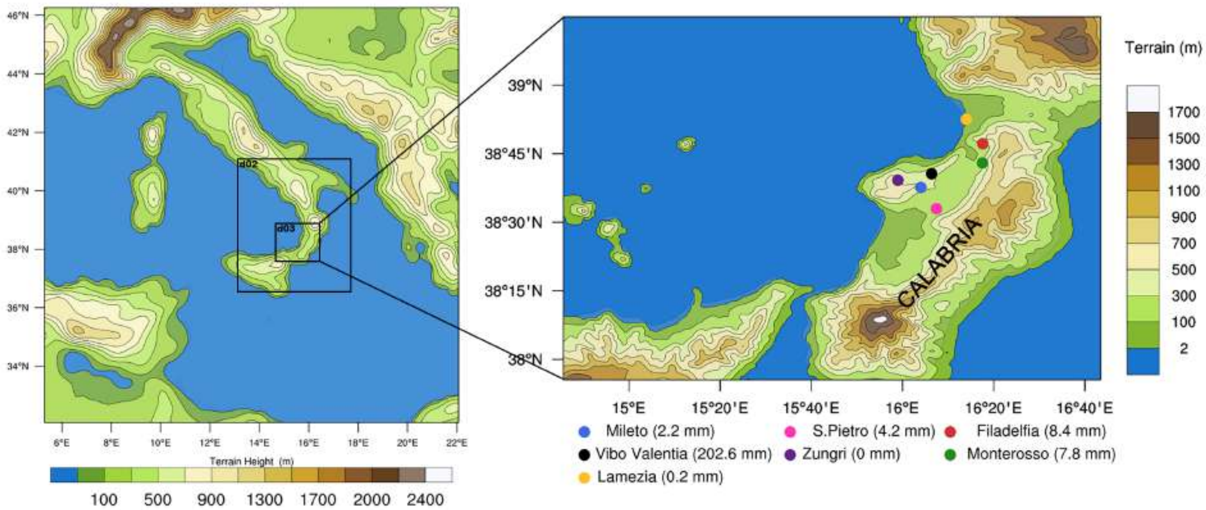

Figure 1: External model domain (D01) and inner domains D02 and D03 defined for WRF model control run (left). Rain gauge network of the Civil Protection of Calabria near Vibo Valentia with 24 h accumulated precipitation on 3 July (right).

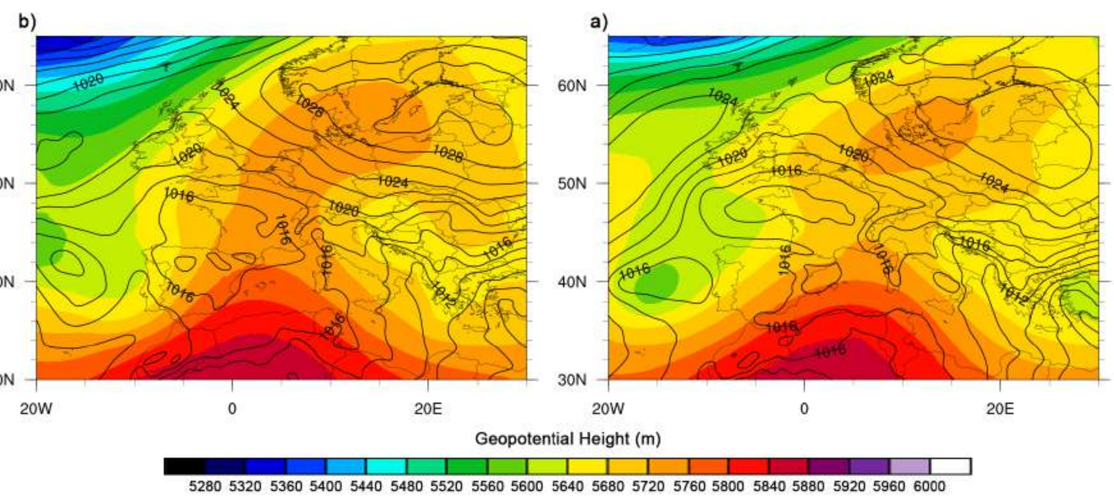

Figure 2: ECMWF analysis of mean sea level pressure (hPa, solid contours) and 500 hPa geopotential height with contours every 40 gpm (m, filled contours) at 1200 UTC 2 July (a) and 1200 UTC 3 July (b).

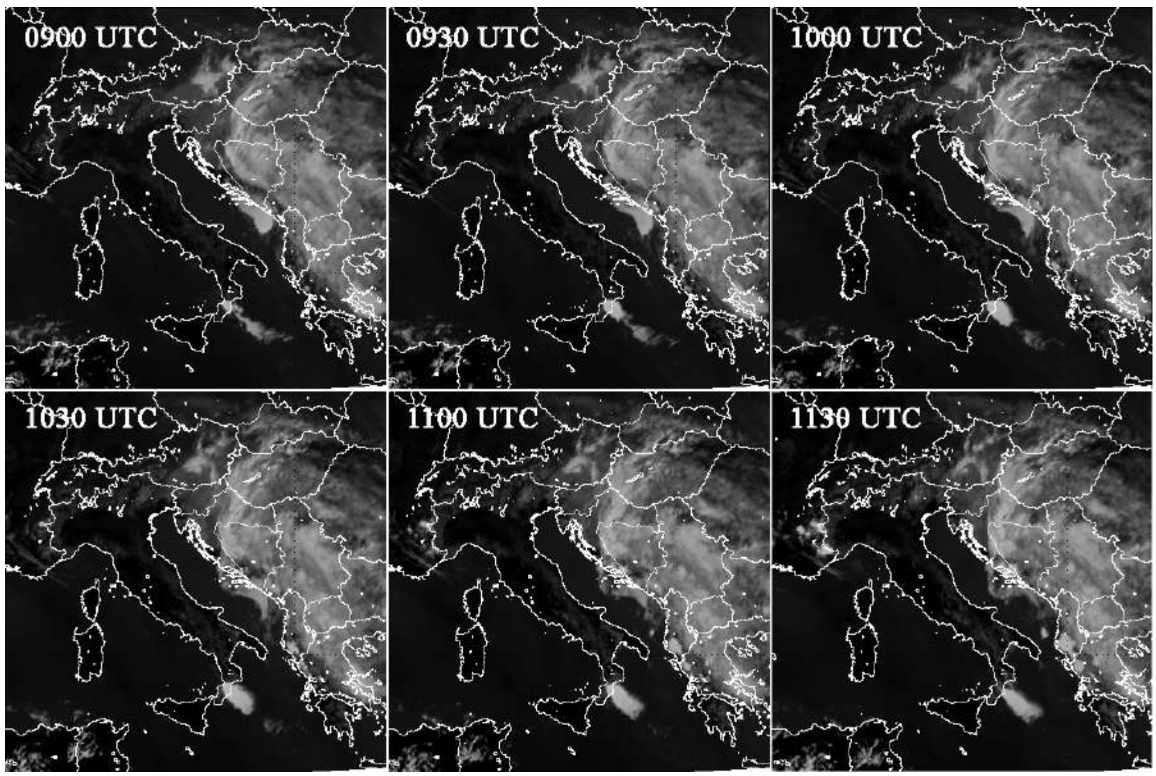

Figure 3: The sequence of 30-minutes MSG brightness temperature at 10.8 μm shows the persistence of convection over Vibo Valentia. The time sequence fits the rain gauge measurements in Chiaravalloti and Gabriele (2009, Fig. 2).

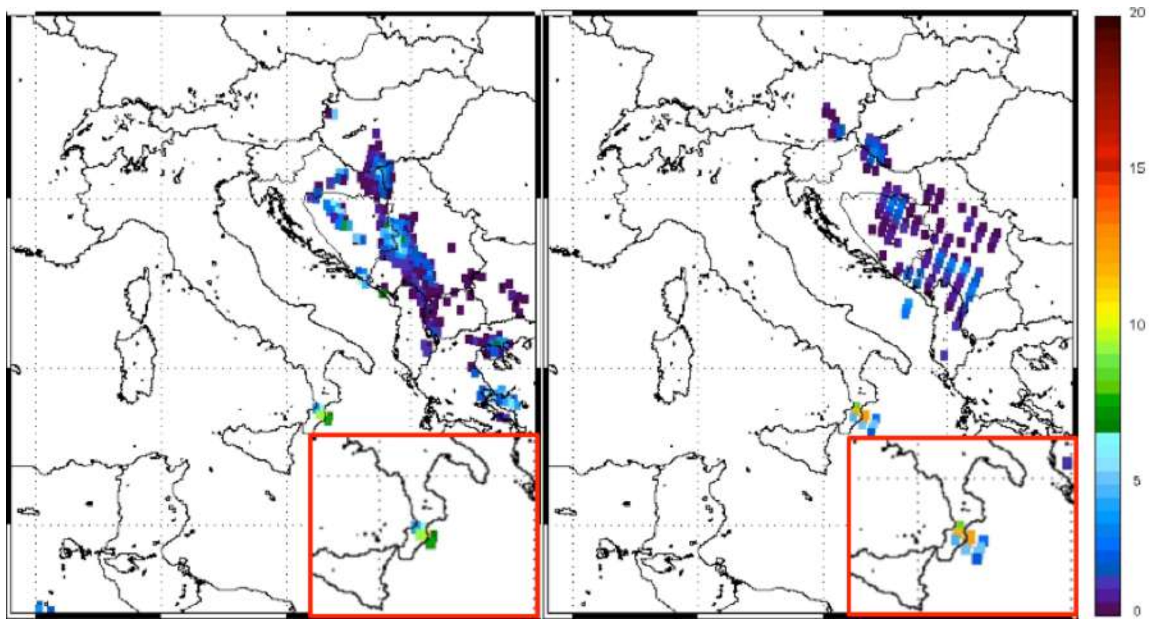

Figure 4: Rain rate retrieval on 3 July 2006 using the 183-WSL method (zoomed in the red square near Vibo). The early morning convection (left panel, 0452 UTC) produces rainfall intensities lower than 10 mm h^{-1}. The intensification of the storm (right panel, 1018 UTC) producing the flooding is responsible for rainfall rates around 15 mm h^{-1}.

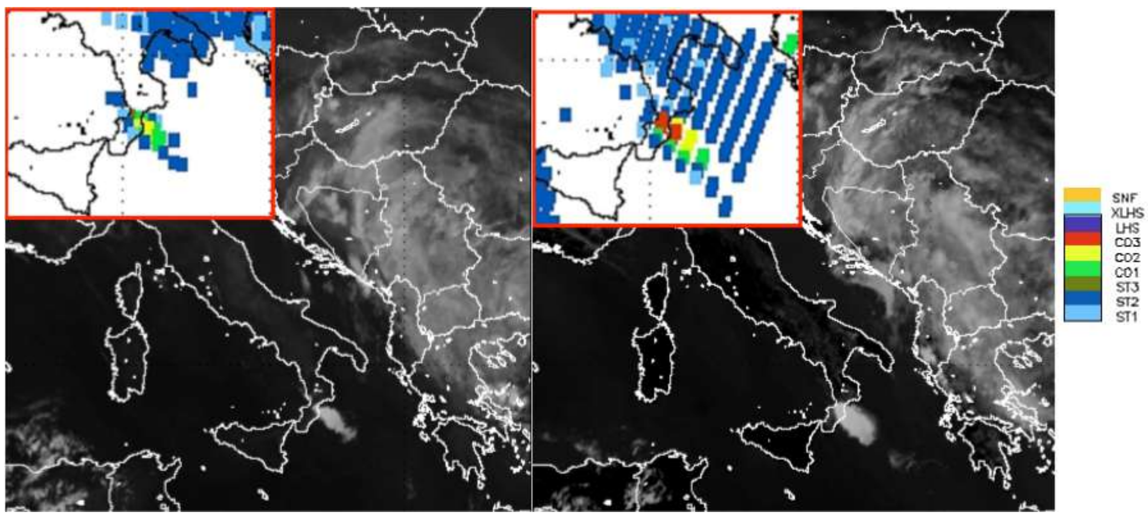

Figure 5: As in Figure 3 but for MSG-SEVIRI channel at 10.8 μm - 0500 UTC (left) and 1030 UTC (right), respectively -. The intensification of convection is described by the MSG brightness temperature values (240 K at 0500 UTC and 210 K at 1030 UTC) and by the MicroWave Cloud Classification (MWCC) method (red square). Legend: ST = Stratiform clouds; CO = Convective clouds; LHS = Large HailStones; XLHS = eXtra Large HailStones; SNF = SNowFall. Both for ST and CO, the category (1, 2, 3) increases with the cloud top altitude. From early morning, the convective system evolves from shallow convection (green and yellow colors) to deep convection (red colour) surrounded by stratiform clouds (blue and cyan).

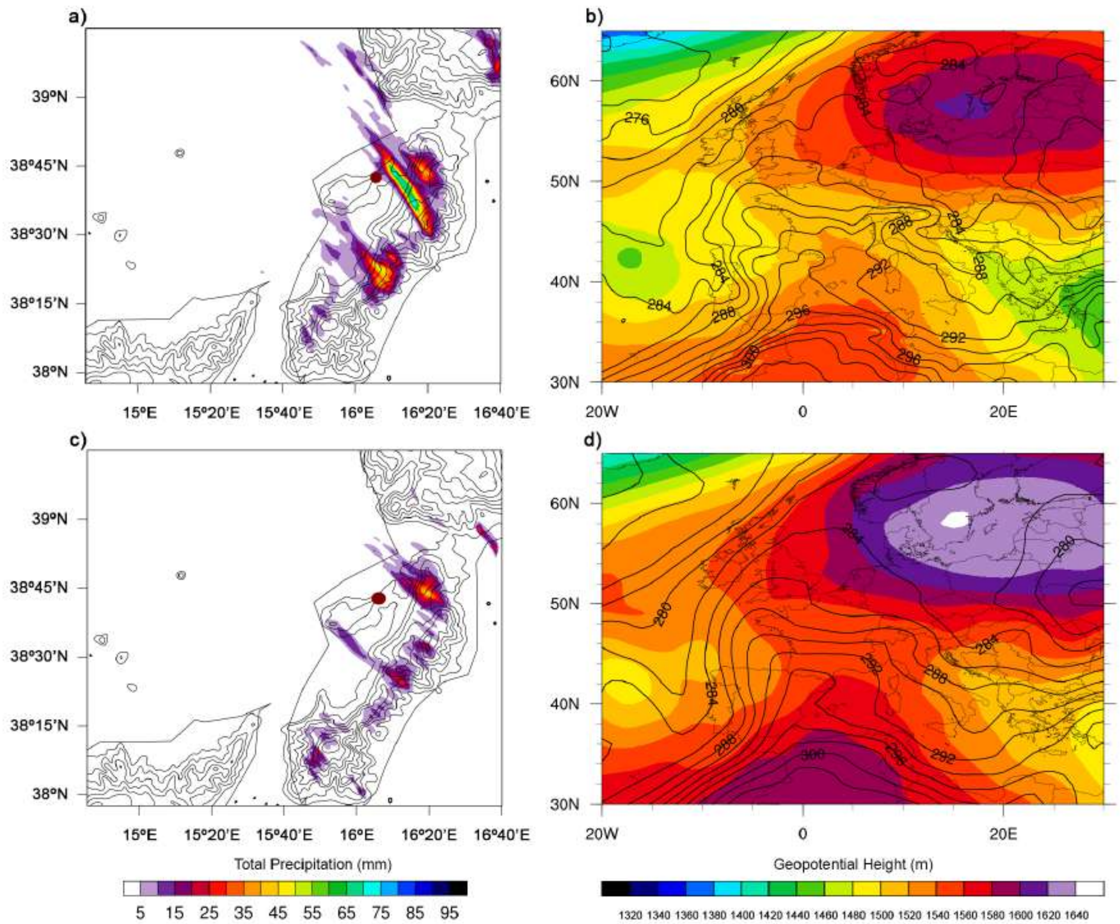

Figure 6: 24 h accumulated precipitation (from 2 July at 1200 to 3 July at 1200) in WRF model, using ECMWF analysis (a) and FNL analysis (c) as initial conditions. 850 hPa temperature (K, solid contours) and geopotential height with contours every 20 gpm (m, filled contours) at 1200 UTC 2 July using ECMWF analysis (b) and FNL analysis (d). The brown point in a) and c) represents the position of Vibo Valentia rain gauge.

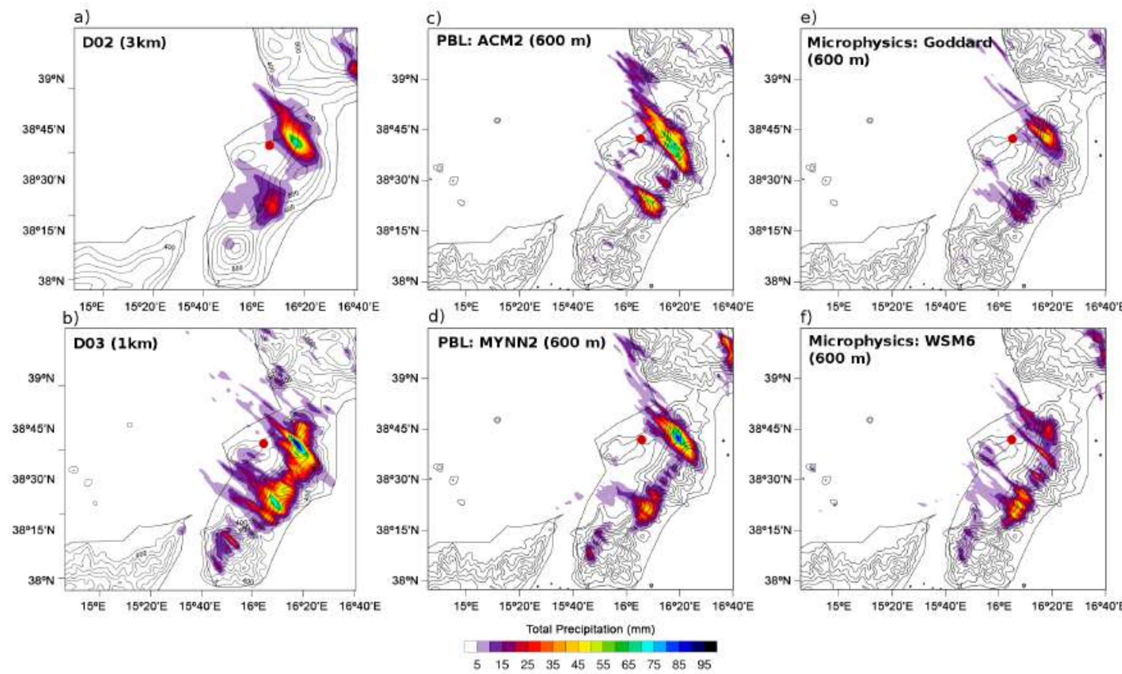

Figure 7: 24 h accumulated precipitation (from 2 July at 1200 to 3 July at 1200) in test runs having: D02 with 3 km horizontal resolution (a), D03 with 1 km horizontal resolution (b), ACM2 PBL scheme (c), MYNN2 PBL scheme (d), Goddard microphysicss scheme (e) and WSM6 microphysics scheme (f). The brown point represents the position of Vibo Valentia rain gauge.

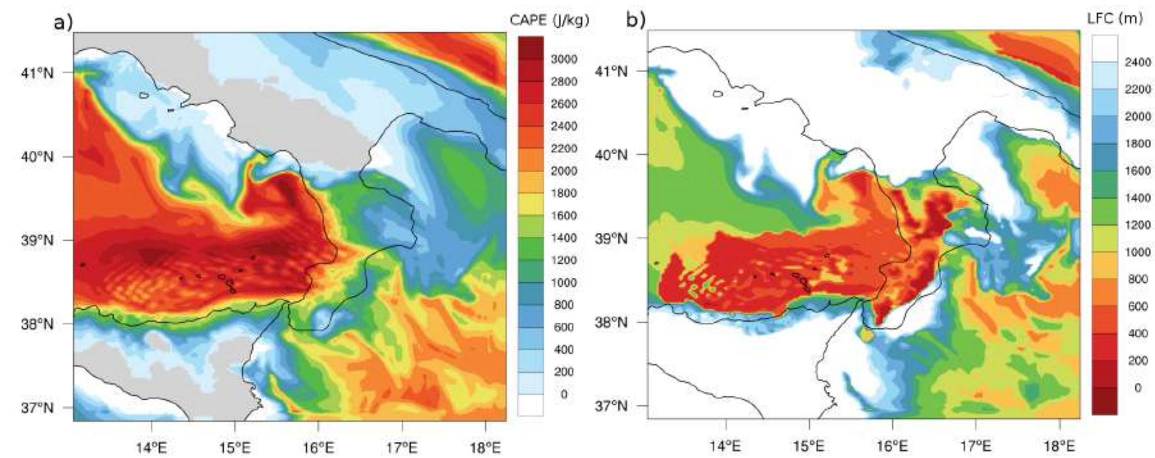

Figure 8: Most unstable CAPE (MCAPE) (in J kg^{-1}, colors) (a) and level of free convection (LFC) (in m, colors) (b) at 0300 UTC 3 July.

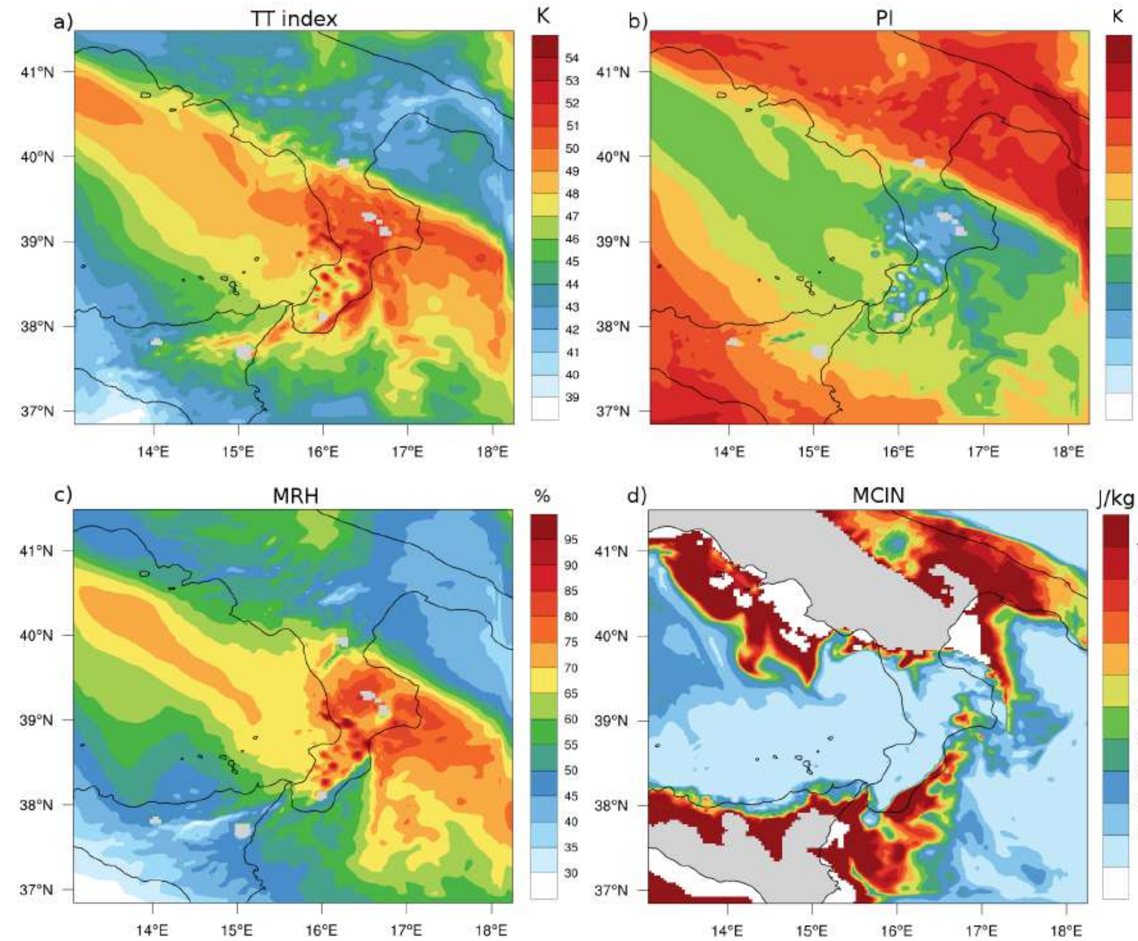

Figure 9: Total totals index (TT) (a), potential instability (PI, in K), mean relative humidity in the lower 300 hPa (MRH, in %) (c) and Most unstable CIN (MCIN, in J kg^{-1}) (d) at 0300 UTC 3 July.

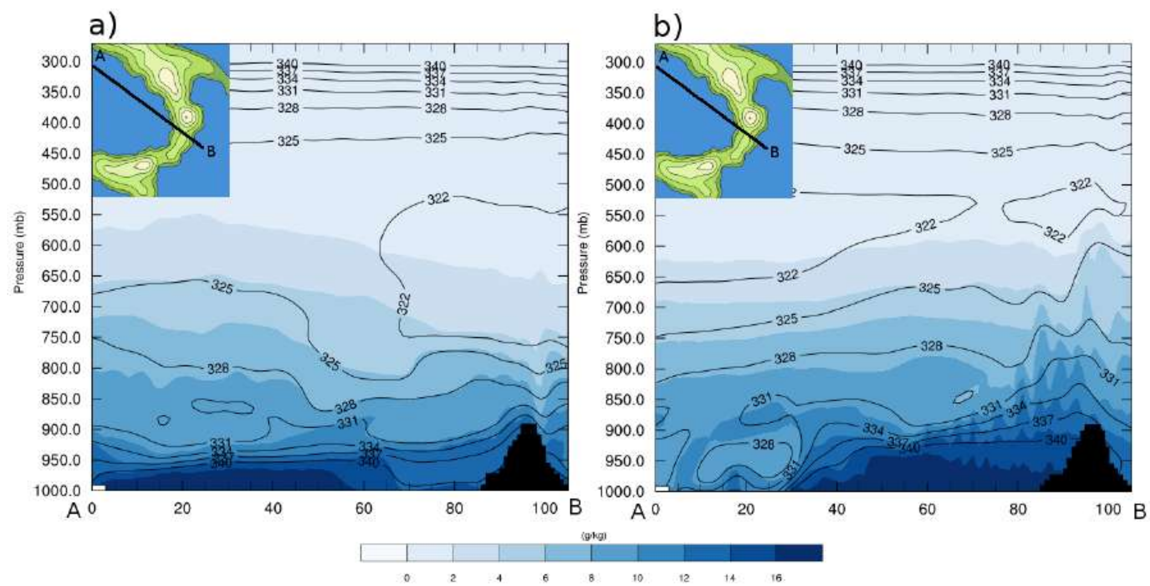

Figure 10: Equivalent potential temperature (θe) (black lines, c.i.= 4 K), and water vapor mixing ratio (colors, c.i.= 2 g kg^{-1}) along a NW-SE cross section in D02 (cross-section line drawn in the upper left corner of the figures) at 1800 UTC 2 July (a) and 0000 UTC 3 July (b) 2006.

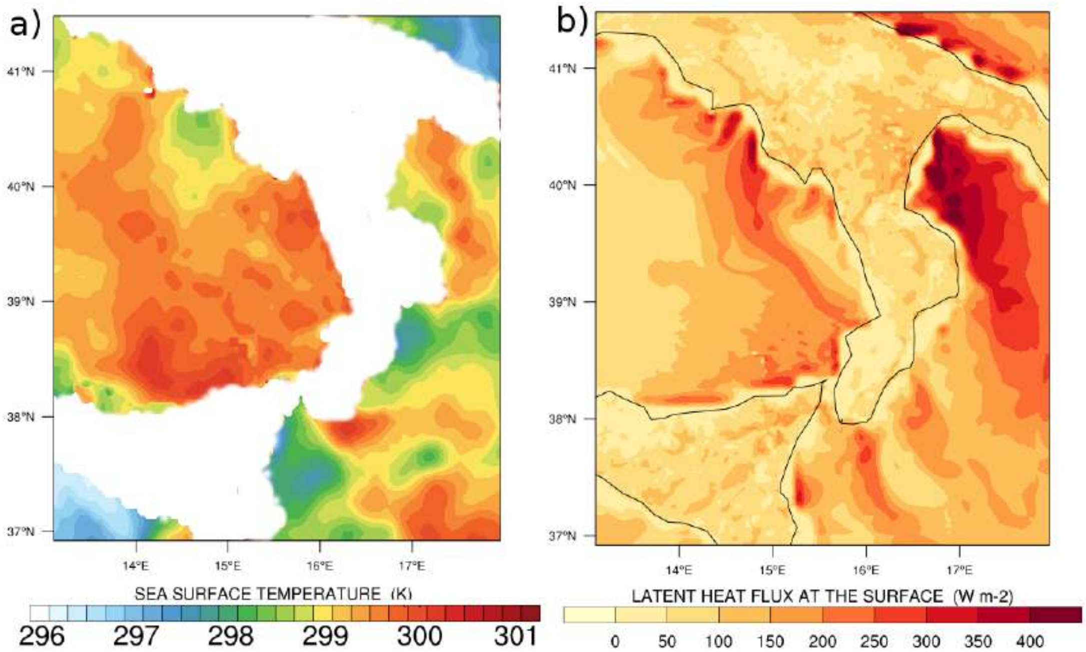

Figure 11: Observed daily averaged sea surface temperature (SST, in K) on 3 July (a) and simulated latent heat flux (LHT, in W m^{-2}) at 0300 UTC 3 July (b).

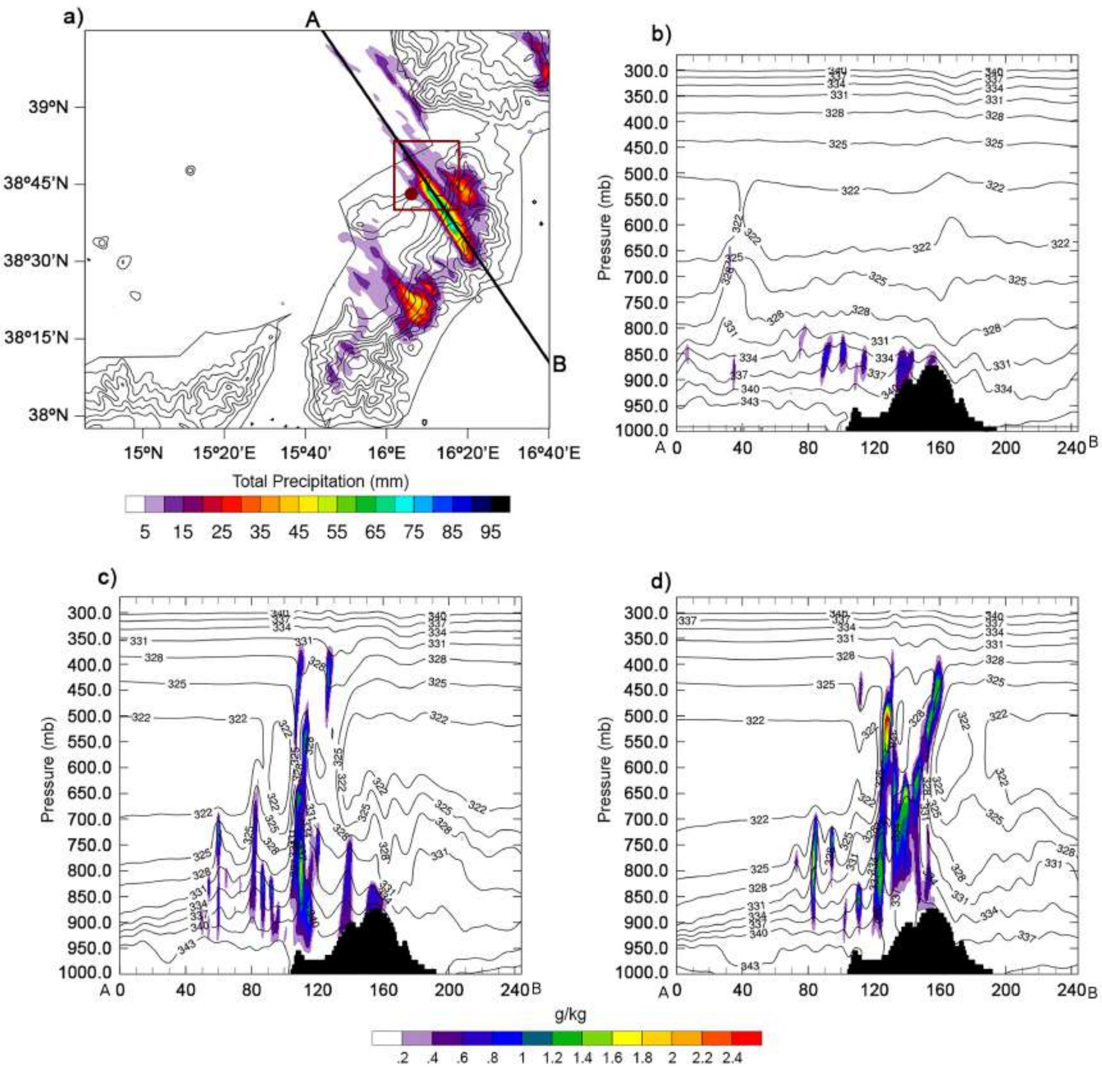

Figure 12: a) Location of cross-section and 24 h accumulated precipitation (from 2 July at 1200 to 3 July at 1200) in D03. The brown frame corresponds to the area represented in Figure 13. The brown point represents the position of the Vibo Valentia rain gauge (a); equivalent potential temperature (θe) (black lines, c.i.= 3 K), and cloud water plus ice content (colors, c.i.= 0.2 g kg^{-1}) along a NW-SE cross section at 0300 UTC (b), 0500 UTC (c) and 0600 UTC (d) 3 July 2006.

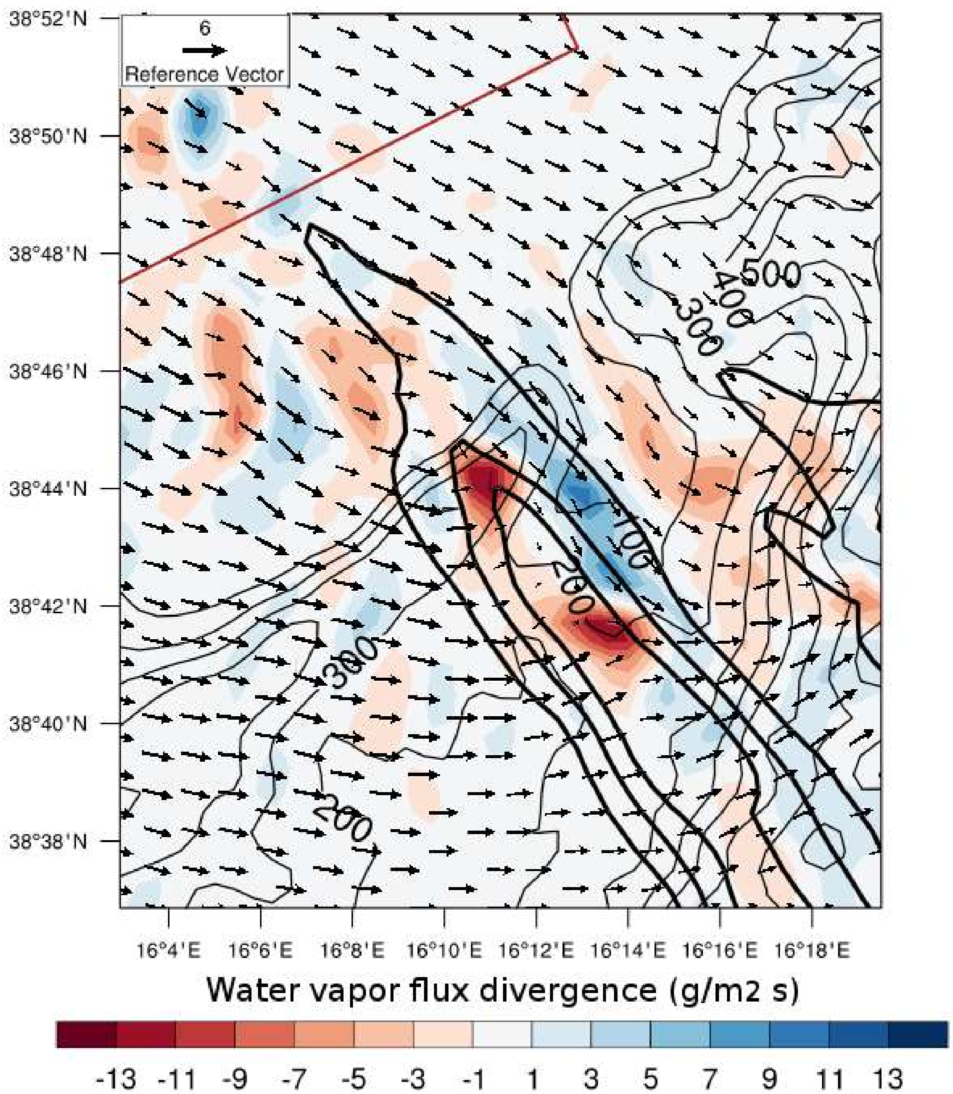

Figure 13: Terrain height (black lines, at 100 m interval), water vapor flux divergence (colors, g m^{-2} s^{-1}) and 925 hPa wind arrows (m s^{-1}) at 0500 UTC 3 July; 24-h accumulated precipitation, from 2 July at 1200 to 3 July at 1200 (black bolded lines, at 20 mm interval). The brown line denotes the coastline.

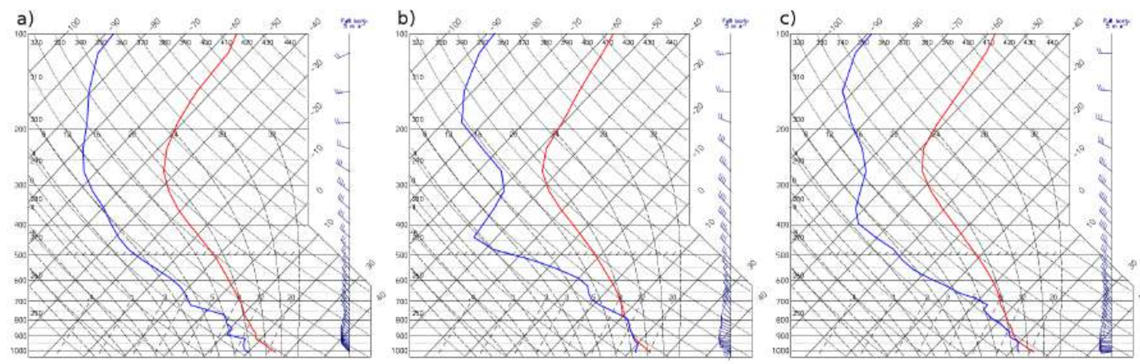

Figure 14: Skew-T diagrams computed from WRF in a location 30 km upstream of the simulated rainfall peak (dewpoint data: blue line, temperature data: red line) at 1800 UTC 2 July (a), 0000 UTC (b) and 0300 UTC (c) 3 July 2006.

Table 1: Table with some instability parameters, calculated 30 km upstream the simulated rainfall peak from 1800 UTC 2 July to 12 UTC 3 July at 3-hours intervals.

Date	U 0-500m (ms^{-1})	Froude	$\frac{h}{LFC}$	$\frac{a/U}{h_{trop}/\sqrt{CAPE}}$
20060702 1800 UTC	4.5	1.0	0.4	7.2
20060702 2100 UTC	5.3	1.2	0.8	6.4
20060703 0000 UTC	4.0	0.9	1.0	8.7
20060703 0300 UTC	5.9	1.5	0.7	5.4
20060703 0600 UTC	6.5	1.7	0.6	4.9
20060703 0900 UTC	6.8	2.1	0.2	2.0
20060703 1200 UTC	6.8	2.3	0.2	2.4